ULTRASONIC COMPUTATION OF DIAMETER DEPENDENT THERMAL PROPERTIES OF InP NANOWIRES

[1]Vimal Pandey, [2]Satyendra Verma, [3]R.R. Yadav
[1]Assistant Professor, [2]Lecturer, [3]Professor
[1]Department of Applied Sciences
[1]United Institute of Technology, Allahabad, India

Abstract : In this paper, we report the diameter dependent ultrasonic characterization of semiconducting InP nanowires having wurtzite structure at the room temperature (300K). In this work, we have calculated higher order elastic constants of InP nanowires validating the interaction potential model depending upon nearest neighbor. The ultrasonic attenuation and velocity in the nanowires are calculated using the higher order elastic constants for different diameters of the nanowires. Finally, we have established the correlation between the size dependent thermal conductivity and the ultrasonic attenuation of the nanowires.

IndexTerms : Ultrasonic Attenuation, Higher Order Elastic Constants, Thermal Conductivity, Thermal Relaxation Time, Semiconducting Nanowires

1. INTRODUCTION

Nanowires of Group III-V semiconductors are well known for their excellent optical and electronic properties. The wurtzite (hexagonal) structured Indium phosphide nanowires (InP NWs) are interesting because of their unique properties such as direct bandgap of 1.35 eV, the highest electron mobility [1], low toxicity, and the smallest effective electron mass. Due to all these properties, InP NWs have their potential application in various fields such as biosensors [2] [3], field effect transistors [4 -7], light- emitting diodes[8], diode laser and infrared detectors [9-11], logic gates [12], photo detectors[13] [14], solar cells[15-17]

A special feature regarding InP NWs is that they have hexagonal closed packed structure or wurtzite structure[18], which is non existing in corresponding bulk material where cubic zinc blend structure prevails [19] [20]**.** Recently zinc blend structured InP NWs are reported to be grown using metal organic vapor phase epitaxy method[21].In wurtzite structured InP NWs each atom has tetrahedral coordination with ABAB stacking sequence which is similar to that in cubic zinc blend structure having c/ a ratio 1.633. In fact the <111> direction for the cubic zinc blend structure is equivalent to the <001> direction of the wurtzite structure[18].The previous studies about crystal structure suggest that the InP NWs with smallest diameter have wurtzite structure while nanowires having large diameter have cubic zinc blend structure[20]. Single crystalline InP NWs having wurtzite structure can be synthesized by chemical beam epitaxy (CBE) [22] and other techniques. The synthesis of these wurtzite structured InP NWs has attracted interest in research fields to determine their electrical and thermal transport properties and their comparison with those of cubic zinc blend structure. However a significant amount of theoretical and experimental work has been focused on investigating mechanical, thermal, electrical and optical properties of wurtzite structured InP NWs but none of the work has been reported in literature so far focused on ultrasonic characterization of InP NWs and to determine their thermal conductivity using ultrasonic evaluation method. The ultrasonic evaluation method is very simple , non-radiative and non-destructive characterization method to predict the microstructural behavior and the thermophysical properties.
In view of this background . in the present work , we have calculated second and third order elastic constants, ultrasonic attenuation and ultrasonic velocity along with related non-linear parameters in InP NWs at 300K aiming to the nondestructive characterization of the materials.

2. THEORY

2.1 SECOND AND THIRD ELASTIC CONSTANTS

According to Brugger [23], elastic constant of n^{th} order is defined as:

$$C_{ijklmn....} = \left(\frac{\partial^n F}{\partial \eta_{ij} \partial \eta_{kl} \partial \eta_{mn} \cdots} \right) \qquad (1)$$

where F is the free energy density of the material and η_{ij} is the Lagrangian strain tensor. The free energy density F of a strained crystal can be expressed in terms of strain tensor η as follows:

$$F = \sum_{n=0}^{\infty} F_n = \sum_{n=0}^{\infty} \frac{1}{n!} \left(\frac{\partial^n F}{\partial \eta_{ij} \partial \eta_{kl} \partial \eta_{mn} \dots} \right) \eta_{ij}\ \eta_{kl}\ \eta_{mn} \dots \quad (2)$$

The second and third order elastic constants,[24-30] of any homogeneous material using above definition can be expressed as

$$C_{IJ} = \partial^2 F / \partial \eta_I \partial \eta_J\ ; \qquad I, J = 1 \dots 6 \quad (3)$$

$$C_{IJK} = \partial^3 F / \partial \eta_I \partial \eta_J \partial \eta_K\ ; \quad I, J, K = 1 \dots 6 \quad (4)$$

where F is free energy density of the material and η is Lagragian strain tensor.

In a hexagonal closed packing (hcp) structured material the unit cell have two types of non-equivalent atoms, six atoms are arranged in basal plane and three-three atoms are above and below the basal plane forming ABABAB….. type structure. The volume of elementary cell is $V_C = \sqrt{3}a^2c/2$, where cell parameters in this structure are a and c.

When ultrasonic waves travel along the unique axis in the material, then the material is deformed homogeneously and deformation factor is given as

$$\rho = \varepsilon_i \varepsilon_j \eta_I \quad (5)$$

where ε_i and ε_j are the cartesian components of position vector r and $\eta_I = \eta_{ij}$ is the Langragian strain tensor. The free energy density of the material F can be expressed in terms of ρ as

$$F = \frac{1}{2V_C}\left[\sum_{I=1}^{6} \frac{1}{2!} \rho^2(I) D^2 \varphi(I) + \sum_{J=1}^{6} \frac{1}{2!} \rho^2(J) D^2 \varphi(J)\right] + \frac{1}{2V_C}\left[\sum_{I=1}^{6} \frac{1}{3!} \rho^3(I) D^3 \varphi(I) + \sum_{J=1}^{6} \frac{1}{3!} \rho^3(J) D^3 \varphi(J)\right] \quad (6)$$

where $D = r^{-1} \frac{d}{dr}$ and φ is interaction potential depending upon nearest neighbor distance r given by,

$$\varphi = -\frac{a_0}{r^m} + \frac{b_0}{r^n} \quad (7)$$

where a_0 and b_0 are constants.

For hexagonal closed packed material equations (3) –(7) leads six second order elastic constant and ten third order elastic constant(TOEC) which are given as,

$C_{11} = 24.1p^4C'$ $C_{12} = 5.918p^4C'$

$C_{13} = 1.925p^6C'$ $C_{33} = 3.464p^8C'$

$C_{44} = 2.309p^4C'$ $C_{66} = 9.851p^4C'$

$C_{111} = 126.9p^2B + 8.853p^4C'$ $C_{112} = 19.168p^2B - 1.61p^4C'$

$C_{113} = 1.924p^4B + 1.155p^6C'$ $C_{123} = 1.617p^4B - 1.155p^6C'$

$C_{133} = 3.695p^6B$ $C_{155} = 1.539p^4B$

$C_{144} = 2.309p^4B$ $C_{344} = 3.464p^6B$

$C_{222} = 101.039p^2B + 9.007p^4C'$ $C_{333} = 5.196p^6B$ (8)

where $p = c/a$ is axial ratio; $C' = \frac{1}{8}[\{nb_0(n-m)\}/\{a^{n+4}\}]\frac{a}{p^5}$ and

$$B = -\frac{1}{8}[\{nb_0(n-m)\}/\{a^{n+4}\}]a^3/\{6a^2(m+n+6)\}p^3$$

The value of parameters $C'$and B is calculated using c, the height of the unit cell, a, the basal plane distance, b_0, Lennard Jones parameter and m, n positive integer numbers called anharmonic parameters.

2.2. ULTRASONIC VELOCITIES

The anisotropic properties of a material are related to ultrasonic velocities in it,which are related to higher-order elastic constants. If ultrasonic wave is propagating along the length of the NWs then there are two types of ultrasonic velocities: one longitudinal and other shear wave velocities [29] [30] which are given by following equations:

$$V_L^2 = C_{33}/\rho \quad (9)$$

$$V_S^2 = C_{44}/\rho \quad (10)$$

where V_L and V_S are longitudinal wave velocity and shear wave velocity respectively and ρ is mass density of the material.

2.3. ULTRASONIC ATTENUATION AND ALLIED PARAMETERS

The main causes for the ultrasonic attenuation in solids are electron-phonon interaction, phonon-phonon interaction, grain boundary loss or scattering loss, Bardoni relaxational loss and thermoelastic loss. The electron mean free path is not comparable to phonon wavelength at room temperature and higher temperatures; therefore attenuation due to electron-phonon interaction will be absent . Scattering loss is prominent for polycrystalline material and it has no role in case of single crystals. Bardoni relaxational loss has been found to be effective at low temperature for metals. So, two dominant processes responsible for the ultrasonic attenuation at room temperature and higher temperatures are phonon-phonon interaction also known as Akhieser loss and thermo-elastic attenuation. The ultrasonic attenuation coefficient due to phonon-phonon interaction or Akhieser loss $(\alpha/f^2)_{Akh}$ mechanism is given by following expression [30]:

$$(\alpha/f^2)_{Akh} = 4\pi^2\tau\Delta C/2dV^3(1+\omega^2\tau^2) \quad (11)$$

where ω is angular frequency of the ultrasonic wave, f is the frequency of the ultrasonic wave; V is the velocity for longitudinal and shear waves as defined in the set of Equations (9) and (10) and ΔC is change in elastic modulus due to variation in strain and is given by expression,

$$\Delta C = 3E_0\langle(\gamma_i^j)^2\rangle - \langle\gamma_i^j\rangle^2 C_v T \quad (12)$$

where E_0 is the thermal energy density and C_v is the specific heat per unit volume of the material [32]; T is the temperature and γ_i^j is Grüneisen number; i and j are the mode and direction of the propagation. The Grüneisen number for a hexagonal WZ structured crystal along the <001> orientation is a direct consequence of the SOECs and TOECs. The acoustic coupling constant "D" is the measure of the acoustic energy converted into thermal energy because when an ultrasonic wave propagates through a crystalline material, the equilibrium of phonon distribution is disturbed, and is given by the equation as:

$$D = 3\Delta C/E_0 \quad (13)$$

. The time taken for re-establishment of equilibrium of the thermal phonons in the crystalline material is termed as the thermal relaxation time "τ" and is given as:

$$\tau = \tau_S = {}^{\tau_L}/_2 = 3K/C_v V_D^2 \quad (14)$$

where τ_L is the thermal relaxation time for the longitudinal wave; is τ_S the thermal relaxation time for the shear wave; and K is the thermal conductivity [33]; $V_D$is the Debye average velocity given by the equation as:

$$V_D = \left[\frac{1}{3}\left(\frac{1}{V_L^3}+\frac{2}{V_S^3}\right)\right]^{-1/3} \quad (15)$$

The propagation of the longitudinal ultrasonic wave results in the thermoelastic loss $(\alpha/f^2)_{Th}$ due to creation of compressions and rarefactions throughout the lattice [30], and it is calculated by the equation given as:

$$(\alpha/f^2)_{Th} = 4\pi^2\langle\gamma_i^j\rangle^2 KT/2\rho V_L^5 \quad (16)$$

The thermoelastic loss for the shear wave has no physical significance because the average of the Grüneisen number for each mode and direction of propagation is equal to zero for the shear wave hence only the longitudinal wave is responsible for thermoelastic loss because it causes variation in entropy along the direction of propagation. The total ultrasonic attenuation is summed up as

$$(\alpha/f^2) = (\alpha/f^2)_{Th} + (\alpha/f^2)_L + (\alpha/f^2)_S \quad (17)$$

where $(\alpha/f^2)_L$ and $(\alpha/f^2)_S$ are the ultrasonic attenuation coefficients due to Akhieser loss for the longitudinal and shear waves respectively.

3. RESULTS AND DISCUSSION

For InP NWs, the unit cell parameters are a = 0.4150 nm, c = 0.6777 nm [25], density d = 4.79 gm/cc and the anharmonic parameters are taken as m =6 and n =7 for wurtzite structured nanowires [33]. The calculated values of second order elastic constants and third order elastic constants (SOEC and TOEC) of InP NWs at 300K using set of equations (6) along with bulk modulus (B), shear modulus (G) , Young's Modulus (Y) and Poisson's ratio (ν), calculated, using the relations for bulk modulus ($B = [2(C_{11} + C_{12}) + 4C_{13} + C_{33}]/9$), shear modulus ($G = [C_{11} + C_{12} + 2C_{33} - 4C_{13} + 12(C_{44} + C_{66})]/30$), Young modulus ($Y = 9BG/(3B+G)$) and Poisson's ratio ($\nu = (3B-2G)/2(3B-G)$), of InP NWs at 300K are given in **Table (1).**

Table 1: Second and third order elastic constants [SOECs (C_{ij}) and TOECs (C_{ijk})], bulk modulus (B), shear modulus (G), Young modulus(Y) in the unit of 10^{10} Nm^{-2} and Poisson's ratio (ν) of InP NWs at 300K.

C_{11}	C_{12}	C_{13}	C_{33}	C_{44}	C_{66}	B	G	Y	ν
126.29	31.00	27.18	131.90	32.62	47.64	61.88	43.39	105.52	0.35
120.3[a]	52.3 [a]	40.7 [a]	131.9 [a]	27.1 [a]	34.0 [a]				
C_{111}	C_{112}	C_{113}	C_{123}	C_{133}	C_{344}	C_{144}	C_{155}	C_{222}	C_{333}
-2059.03	-326.48	-69.77	-88.61	-445.53	-417.68	-103.29	-68.86	-1629.09	-1689.01

[a] Reference [25]

Thermal energy density (E_0) and specific heat per unit volume (C_V), longitudinal wave velocity (V_L), shear wave velocity (V_S) and Debye average velocity (V_D) have been calculated with the help equations (7), (8), (13), and literature [25] along with acoustic coupling constants for InP NWs at 300K are calculated using equations (10) and (11) are shown in **Table (2)**.

Table 2: Thermal energy density (E_0), specific heat per unit volume (C_V), ultrasonic velocities (V_L, V_S and V_D) along <001> direction and acoustic coupling constant (D_L and D_S) for InP NWs at 300K.

E_0 ($x10^8 Jm^{-3}$)	C_V ($x\ 10^6\ JK^{-1}m^{-3}$)	V_L ($x\ 10^3 ms^{-1}$)	Vs ($x\ 10^3 ms^{-1}$)	V_D ($x\ 10^3 ms^{-1}$)	D_L	Ds
1.733	0.793	5.24	2.60	2.89	10.328	0.483

The Grüneisen number which are direct consequences of the SOEC and the TOEC, for InP NWs at 300 K are given in **Table (3)**.

Table 3: Grüneisen numbers of InP NWs at 300K

$\langle\gamma_i^j\rangle_L$	$\langle(\gamma_i^j)^2\rangle_L$	$\langle\gamma_i^j\rangle^2{}_L$	$\langle\gamma_i^j\rangle_S$	$\langle(\gamma_i^j)^2\rangle_S$	$\langle\gamma_i^j\rangle^2{}_S$
-0.2557	1.1774	0.0654	0	0.0536	0

Size (diameter) dependent thermal conductivities of InP NWs are taken from the literature [25]; size dependent thermal relaxation time (τ) along unique axis of InP NWs is calculated using equation (12) at 300 K; ultrasonic attenuation coefficients over square of frequency (α/f^2) for longitudinal and shear wave due to phonon-phonon interaction (Akhieser loss) and thermoelastic relaxation mechanisms for InP NWs are calculated using equations (9) and (14) at 300K respectively under the

condition □□<<1 and total ultrasonic attenuation over square of frequency, $(\alpha/f^2)_{Total}$ calculated using equation (15) at 300K under the condition □□<<1 are given in **Table (4)**.

Table 4: Diameter dependent thermal conductivity (K), relaxation time (τ),thermoelastic loss $(\alpha/f^2)_{Th}$ and ultrasonic attenuation over square of frequency (α/f^2) for longitudinal $[(\alpha/f^2)_{Akh.\ Long.}]$ and shear wave $[(\alpha/f^2)_{Akh.\ Shear}]$ and total ultrasonic attenuation over square of frequency $(\alpha/f^2)_{Total}$ for InP NWs at 300K.

d (nm)	K ($Wm^{-1}K^{-1}$)	τ ($x10^{-12}$ s)	$(\alpha/f^2)_{Th}$ ($x10^{-22}Np\ s^2m^{-1}$)	$(\alpha/f^2)_{Akh.\ Long.}$ ($x10^{-19}Np\ s^2m^{-1}$)	$(\alpha/f^2)_{Akh.\ Shear}$ ($x10^{-19}Np\ s^2m^{-1}$)	$(\alpha/f^2)_{Total.}$ ($x10^{-19}Np\ s^2m^{-1}$)
1.66	2.11	0.964	4.24	6.57	1.25	7.82
2.49	2.00	0.909	4.08	6.19	1.18	7.37
3.32	2.35	1.068	4.80	7.28	1.38	8.66
4.15	2.38	1.082	4.86	7.37	1.40	8.77
4.97	2.65	1.204	5.41	8.20	1.56	9.76

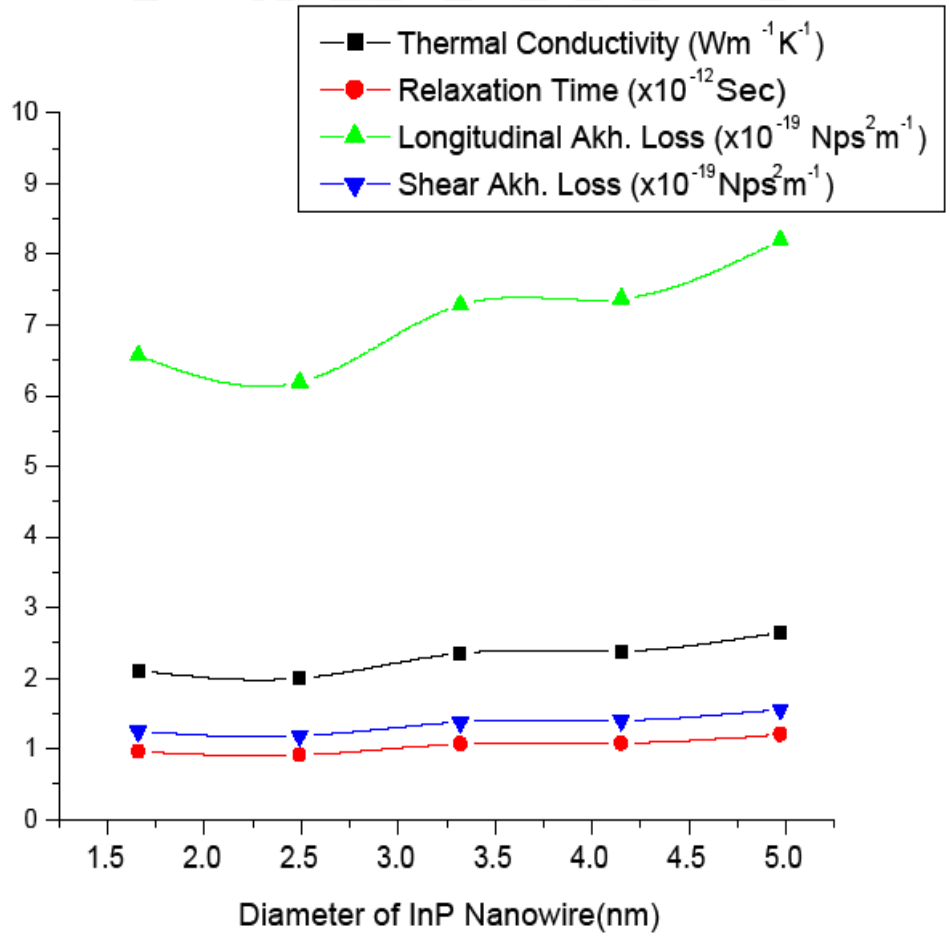

Figure 1. Thermal Conductivity, relaxation time, longitudinal Akhiser loss and shear Akhiser loss vs diameter of InP nanowire.

The calculated values of SOECs at 300 K based on lattice parameters using the simple interaction potential are compared in **Table 1**, which shows that both the results are in good agreement with 10-20% variation. Thus our theoretical approach for the calculation of SOEC/TOEC for InP nanowires at room temperature is validated.

The acoustic coupling constant are related to conversion of acoustic energy into thermal energy as the ultrasonic wave propagates in the nanowire. For the longitudinal wave D_L is greater than that for the shear wave D_S this is seen in InP nanowire from perusal of **Table 2**. Acoustic coupling constant D_L, for longitudinal ultrasonic wave and acoustic coupling constant D_S, for shear ultrasonic wave in various sized (1.66nm, 2.49nm, 3.32nm, 4.15nm, 4.97nm) InP NWs are 10.328 and 0.483 respectively. In nanowires number of atoms at surface is less than that the number of atoms/particles in the volume in both hexagonal (wurtzite) structure and zinc blende structure. Thus in hexagonal structured InP nanowires the interaction of longitudinal acoustical phonon with thermal phonon of medium will be larger than that of shear. This is the reason behind the obtaining high acoustic coupling constant D_L than D_S.

Finally we have determined the ultrasonic attenuation using the calculated SOECs and TOECs. The ultrasonic attenuation for longitudinal wave $(\alpha/f^2)_{\text{Long.}}$ is greater than that for shear wave $(\alpha/f^2)_{\text{Shear}}$, as is observed from perusal of **Table 4**. The Akhiser loss is proportional to thermal relaxation time (τ). Since the ultrasonic velocity is directly related to elastic constant, this implies that the Akhiser loss in the nanowire is affected by elastic constant and thermal relaxation time. The thermoelastic loss is directly related to thermal conductivity of nanowires and is very small in comparision to Akhiser loss as observed from **Table 4**. A plot of thermal conductivity, relaxation time, longitudinal Akhiser loss and shear Akhiser loss with diameter of InP nanowire is given in **Figure 1.** It is also clear that ultrasonic attenuation (longitudinal Akhiser loss and shear Akhiser loss) varies with diameter accordingly as the thermal conductivity varies with the diameter.

The plots of τ and (α/f^2) have similar nature as thermal conductivity (K) have with diameter of nanowire. The Akhiser loss in longitudinal wave is dominating thus total ultrasonic attenuation $(\alpha/f^2)_{\text{Total}}$ in InP nanowire is mainly governed by the loss due to phonon-phonon interaction.

4. CONCLUSIONS

The simple interaction potential model for the calculation of second and third order elastic constants is validated for the nanowires of different diameters. Theoretical approach for the determination of ultrasonic attenuation in nanowires at 300 K with different diameters is established. There is strong correlation between ultrasonic attenuation and thermal conductivity in the nanowires. Thus ultrasonic attenuation method can be used to extract the important information about the microstructural phenomena like phonon-phonon interaction in the nanowires and thermal conductivity behavior with respect to diameter of the nanowire.

REFERENCES

[1] Sun, J., Yin, Y,, Han, M., Yang, Z.X., Lan, C., Liu, L., Wang, Y., Han, N., Shen, L., Wu, X., Ho, J.C. (2018), Nonpolar-Oriented Wurtzite InP Nanowires with Electron Mobility Approaching the Theoretical Limit, ACS Nano, 12(10), 10410-10418.
[2] Cui, Y., Wei, Q., Park, H. and Lieber, C.M. (2001) Nanowire Nanosensors for Highly Sensitive and Selective Detection of Biological and Chemical Species, Science, **293**, 1289-1292.
[3] Hahm, J. and Lieber, C.M. (2004) Direct Ultrasensitive Electrical Detection of DNA and DNA Sequence Variations Using Nanowire Nanosensors, Nano Letters, **4**, 51-54.
[4] Duan, X., Huang, Y., Cui, Y., Wang, J. and Lieber, C.M. (2001) Indium Phosphide Nanowires as Building Blocks for Nanoscale Electronic and Optoelectronic Devices, Nature, **409**, 66-69.
[5] Cui, Y., Zhong, Z., Wang, D., Wang, W.U. and Lieber, C.M. (2003) High Performance Silicon Nanowire Field Effect Transistors, Nano Letters, **3**, 149-152.
[6] Ng, H.T., Han, J., Yamada, T., Nguyen, P., Chen, Y.P. and Meyyappan, M. (2004) Single Crystal Nanowire Vertical Surround-Gate Field-Effect Transistor. Nano Letters, **4**, 1247-1452.
[7] Persson, A.I., Björk, M.T., Jeppesen, S., Wagner, J.B., Wallenberg, L.R. and Samuelson, L. (2006) InAs1-*x*P*x* Nanowires for Device Engineering, Nano Letters, **6**, 403-407.
[8] Park, H., Barrelet, C.J., Wu, Y., Tian, B., Qian, F. and Lieber, C.M. (2008) A Wavelength-Selective Photonic-Crystal Waveguide Coupled to a Nanowire Light Source. Nature Photonics, **2**, 622-626.
[9] Gong, X.Y., Kan, H., Makino, T., Yamaguchi, T., Nakatskasa, T., Kumagawa, M., Rowell, N.L., Wang, A. and Rinfret, R. (1995) High Quality InAs1–*y*Sby/InAs Multilayers for Mid-IR Detectors. Crystal Research & Technology, **30**, 603-612.
[10] Shenoi, R.V., Attaluri, R.S., Siroya, A., Shao, J., Sharma, Y.D., Stintz, A., Vandervelde, T.E. and Krishna, S. (2008) Low-Strain InAs/InGaAs/GaAs Quantum Dots-in-a-Well Infrared Photodetector. Journal of Vacuum Science & Technology B, **26**, 1136-1139.
[11] Mou, S., Petschke, A., Lou, Q., Chuang, S.L., Li, J.V. and Hill, C.J. (2008) Midinfrared InAs/GaSb Type-II Superlattice Interband Tunneling Photodetectors, Applied Physics Letters, **92**, Article ID: 153505.

[12] Huang, Y., Duan, X., Cui, Y., Lauhon, L.J., Kim, K. and Lieber, C.M. (2001) Logic Gates and Computation from Assembled Nanowire Building Blocks. Science, **294**, 1313-1317.
[13] Wang, J., Gudiksen, M.S., Duan, X., Cui, Y. and Lieber, C.M. (2001) Highly Polarized Photoluminescence and Photodetection from Single Indium Phosphide Nanowires, Science, **293**, 1455-1457.
[14] Pettersson, H., Trägårdh, J., Persson, A.I., Landin, L., Hessman, D. and Samuelson, L. (2006) Infrared Photodetectors in Heterostructure Nanowires, Nano Letters, **6**, 229-232.
[15] Law, M., Greene, L.E., Johnson, J.C., Saykally, R. and Yang, P. (2005) Nanowire Dye-Sensitized Solar Cells. Nature Materials, 4, 455-459.
[16] Dan Wu, Xiaohong Tang, Kai Wang, Zhubing He and Xianqiang Li, (2017), An Efficient and Effective Design of InP Nanowires for Maximal Solar Energy Harvesting, Nanoscale Research Letters 12(604).
[17] Wallentin, Nicklas Anttu, Damir Asoli, Maria Huffman, Ingvar Åberg, Martin H. Magnusson, Gerald Siefer, Peter Fuss-Kailuweit, Frank Dimroth, Bernd Witzigmann, H. Q. Xu, Lars Samuelson, Knut Deppert, Magnus T. Borgström, (2013), InP Nanowire Array Solar Cells Achieving 13.8% Efficiency by Exceeding the Ray Optics Limit, Science, 339(6123),1057-1060.
[18] Xulu Zeng, Gaute Otnes, Magnus Heurlin, Renato T Mourão, and Magnus T Borgström (2018), InP/GaInP nanowire tunnel diodes, Nano Research, 11(5): 2523–2531.
[19] Zhou, F. (2009) Thermoelectric Transport in Semiconducting Nanowires. Ph.D. Dissertation, The University of Texas, Austin.
[20] Caroff, P., Dick, K.A., Johansson, J., Messing, M.E., Deppert, K. and Samuelson, L. (2009) Controlled Polytypic and Twin-Plane Superlattices in III-V Nanowires, Nature Nanotechnology, **4**, 50-55.
[21] Krishnamachari, U., Borgstrom, M. , Ohlsson, B. J. , Panev, N. , Samuelson, L. , and Seifert, W. (2004). Defect free InP nanowires grown in [001] direction on InP substrate**,** Appl. Phys. Lett. 85,2077.
[22] Persson, A.I., Froberg, L.E., Jeppesen, S., Bjork, M.T. and Samuelson, L. (2007) Surface Diffusion Effects on Growth of Nanowires by Chemical Beam Epitaxy. Journal of Applied Physics, **101**, Article ID: 034313.
[23] Zhang, J., Zhang, L.D., Wang, X.F., Liang, C.H., Peng, X.S., Wang, Y.W. (2001**)** Fabrication and Photoluminescence of Ordered GaN Nanowire Array. Journal of Chemical Physics, **115 (13), 5714**.
[24] Yadav, A.K., Yadav, R.R., Pandey, D.K. and Singh, D. (2008) Ultrasonic Study of Fission Products Precipitated in the Nuclear Fuel. Materials Letters, **62**, 3258-3261.
[25] Sindhu, S. and Menon, C.S. (1995) Fourth Order Nonlinear Elastic Coefficient of Hexagonal Close Packed Lattice.Journal of Physics and Chemistry of Solids, **57**, 1307-1309.
[26] Verma, S.K., Pandey, D.K. and Yadav, R.R. (2012) Size Dependent Ultrasonic Properties of InN Nanowires. Physica B: Condensed Matter, **407**, 3731-3735.
[27] Dhawan, P.K., Wan, M., Verma, S.K., Pandey, D.K. and Yadav, R.R. (2015) Effect of Diameter and Surface Roughness on Ultrasonic Properties of GaAs Nanowires. Journal of Applied Physics, **117**, Article ID: 074307.
[28] Pandey, D.K., Yadawa, P.K. and Yadav, R.R. (2007) Ultrasonic Properties of Hexagonal ZnS at Nanoscale. Materials Letters, **61**, 5194-5198.
[29] Pandey, D.K., Singh, D. and Yadav, R.R. (2007) Ultrasonic Wave Propagation in 3rd Group Nitrides. Applied Acoustics, **68**, 766-777.
[30] Larsson, M.W., Wagner, J. B., Wallin, M., Håkansson P., Fröberg, L. E., Samuelson, L., and Wallenberg L.R., (2007), Strain Mapping in Free-Standing Heterostructured Wurtzite InAs/InP Nanowires, Nanotechnology, 18 (015504).
[31] Gray, D.E. (1972) American Institute of Physics Handbook. 3rd Edition, McGraw-Hill, New York, 4-58.
[32] Carrete, J., Longo, R.C. and Gallego, L.J. (2011) Prediction of Phonon Thermal Transport in Thin GaAs, InAs and InP Nnowires by Molecular Dynamics Simulations Influence of the Interatomic Potential. Nanotechnology, **22**, Article ID: 185704.